Discover Applied Sciences

RESEARCH Open Access

Modeling of solar photovoltaic generation and power conditioning systems using maxwell's equations of electromagnetics

M. M. Mundu[1*], Mariam Basajja[2], Emmanuel Kweyu[3], J. I. Ssempewo[4], S. N. Nnamchi[5] and Daniel Ejim Uti[6*]

*Correspondence:
M. M. Mundu
mundu.mustafa@kiu.ac.ug
Daniel Ejim Uti
daniel.ejimuti@kiu.ac.ug; dan4uti@gmail.com

Full list of author information is available at the end of the article

Abstract

Accurate modeling of photovoltaic (PV) systems coupled with power conditioning inverters is critical for optimizing efficiency, reliability, and thermal performance, especially in high-frequency and high-penetration applications. This study presents a Maxwell-based electromagnetic simulation framework that integrates PV module field distributions with inverter electromagnetic behavior, enabling a physically consistent evaluation of electric and magnetic stresses, losses, and thermal effects. Spatially resolved simulations reveal localized electric field hotspots, magnetic flux concentrations, and parasitic loss mechanisms that are not captured by conventional lumped-parameter models. Sensitivity analysis confirms the numerical stability and robustness of the coupled field–circuit model under variations in mesh, time-step, and material properties. Results demonstrate enhanced prediction of efficiency, component stress, and thermal behavior, offering actionable insights for inverter and PV design optimization. The proposed methodology supports reliable deployment of mini-grid and high-penetration PV systems, contributing to Sustainable Development Goals (SDG 7 and SDG 13) and advancing renewable energy strategies in African and emerging energy markets.

Keywords Photovoltaic systems, Maxwell's equations, Electromagnetic modeling, Power conditioning inverters, Finite-element simulation, Renewable energy, Sustainable energy deployment

1 Introduction

The increasing integration of solar PV systems into modern energy grids demands precise modeling and simulation to accurately predict energy generation and power conversion. Traditional lumped-parameter or quasi-static PV models, while computationally efficient, often overlook detailed electromagnetic phenomena such as displacement currents, field non-uniformities, and parasitic effects, which become significant in high-frequency inverter operations and impact system efficiency and reliability [1–4]. Advanced modeling approaches include detailed single-diode equivalent circuit models that adjust parameters based on key points like open circuit, maximum power, and short circuit to

© The Author(s) 2026. **Open Access** This article is licensed under a Creative Commons Attribution-NonCommercial-NoDerivatives 4.0 International License, which permits any non-commercial use, sharing, distribution and reproduction in any medium or format, as long as you give appropriate credit to the original author(s) and the source, provide a link to the Creative Commons licence, and indicate if you modified the licensed material. You do not have permission under this licence to share adapted material derived from this article or parts of it. The images or other third party material in this article are included in the article's Creative Commons licence, unless indicated otherwise in a credit line to the material. If material is not included in the article's Creative Commons licence and your intended use is not permitted by statutory regulation or exceeds the permitted use, you will need to obtain permission directly from the copyright holder. To view a copy of this licence, visit http://creativecommons.org/licenses/by-nc-nd/4.0/.

closely match real PV array behavior, enabling accurate simulation of I-V characteristics and power output ([3]; et al., 2019). Artificial intelligence techniques such as artificial neural networks, fuzzy logic, and genetic algorithms have also been extensively applied to improve performance prediction, maximum power point tracking, and fault detection, offering robust tools to handle uncertainties in solar radiation and environmental conditions [5, 6]. For grid integration, simulation of three-phase PV systems with control schemes including MPPT algorithms and PWM inverters is essential to ensure synchronization and efficient power flow between PV arrays and the grid [7–10]. Simplified yet accurate models that balance computational speed and fidelity are critical for long-term and large-scale PV system analyses, facilitating design optimization and operational management in diverse climatic and geographic settings [4, 11].

Despite the critical role of electromagnetic phenomena in PV systems, there is a notable lack of research applying Maxwell's equations directly to PV system modeling. Most existing studies model PV arrays and inverters as idealized circuit elements, using equivalent electrical circuits or simplified mathematical models that do not capture the underlying field interactions [12–15]. This simplification leads to underestimation of losses, inability to predict localized electrical stresses, and neglect of displacement currents and parasitic effects that influence long-term reliability and energy yield. While some work clarifies power flow in polyphase systems using Poynting's vector derived from Maxwell's equations, these approaches have not been widely extended to detailed PV system simulations [16]. Instead, the majority of PV modeling relies on nonlinear circuit equations or state-space methods that focus on electrical output characteristics rather than electromagnetic field distributions [13, 17, 18]. Addressing this gap by integrating Maxwell's equations into PV system models could improve accuracy in predicting efficiency, losses, and component degradation, especially under high-frequency inverter operation and complex environmental conditions.

To address these limitations, this study present a Maxwell-based electromagnetic modeling framework for solar PV generation and power conditioning systems by integrating fundamental electromagnetic laws directly into simulations to capture detailed electric and magnetic field distributions, displacement currents, and high-frequency switching effects. Such an approach enables precise analysis of field effects on system efficiency, loss mechanisms, and reliability without relying on experimental field data. Existing electromagnetic transient (EMT) simulation tools like ATP-EMTP and PSCAD/EMTDC have been used to model PV systems and their grid interfaces, incorporating inverter controls and transient behaviors to evaluate performance and protection under normal and fault conditions [19, 20]. Advanced models also address power converter dynamics using state-space averaging methods to balance accuracy and computational efficiency, reflecting steady-state and transient characteristics of PV inverters [21]. Recent frameworks extend to multiphysics modeling, coupling electromagnetic, electrical, and thermal behaviors to assess parasitic effects, switching losses, and temperature-dependent performance in power conversion systems [22]. Large-scale PV system simulations leverage GPU-CPU parallel architectures to handle detailed nonlinear transient modeling of millions of PV panels, enabling scalable and efficient electromagnetic transient analysis in integrated AC/DC grids [23]. Together, these developments support the proposed Maxwell-based framework's goal of capturing complex electromagnetic interactions in PV systems for improved simulation fidelity and system design.

Moreover, photovoltaic modeling approaches generally fall into three categories. The first comprises semiconductor device models, such as drift–diffusion formulations, used to analyze carrier dynamics and recombination within PV cells. The second includes circuit-level models in which PV modules are represented using equivalent circuits typically single- or double-diode models combined with inverter representations to evaluate power conversion efficiency and system dynamics. These diode-based models remain the most widely used, with parameter extraction being an active research area aimed at improving prediction accuracy under varying environmental conditions [24, 25]. Recent developments include iterative and explicit techniques that simplify parameter extraction without solving implicit equations, improving computational efficiency while maintaining accuracy [26, 27]. Artificial intelligence methods such as neural networks, fuzzy logic, and genetic algorithms have also been applied to address uncertainties in PV performance prediction and parameter estimation [5], while metaheuristic algorithms have demonstrated strong capability for extracting parameters from nonlinear PV models across diverse operating conditions [28, 29]. A third category involves electromagnetic field-based models derived from Maxwell's equations, traditionally applied to component-level analysis of power electronic devices and magnetic structures rather than integrated PV–inverter systems. Together, these approaches support improved simulation fidelity and system design by capturing electrical, thermal, optical, and electromagnetic interactions in PV systems [3, 30].

Thus, the key contributions of this work include the development of a Maxwell-consistent electromagnetic model for PV generation and inverter-based power conditioning systems, enabling direct simulation of electric and magnetic field interactions within the system. The implementation of this simulation framework allows evaluation of electromagnetic field impacts on energy conversion efficiency, electrical losses, and stress indicators, capturing phenomena often neglected by conventional lumped circuit models [20, 21, 31]. A quantitative comparison between traditional lumped parameter models and the proposed field-based simulations demonstrates improved predictive accuracy, particularly in representing high-frequency switching effects and localized electromagnetic stresses that affect reliability and performance [32–35].

Figure 1 conceptually illustrates the system layout, showing the PV array, inverter, and load components, with electric ($\vec{E}$) and magnetic ($\vec{B}$) fields depicted around the inverter and power conditioning elements, emphasizing the spatial distribution

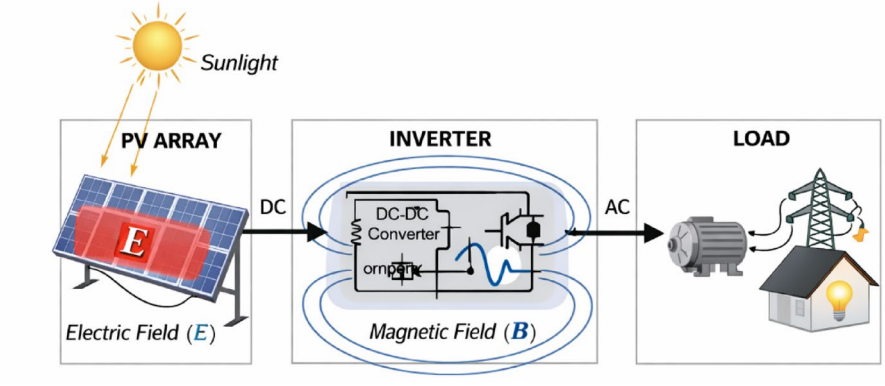


Fig. 1 Conceptual Schematic of the Solar Photovoltaic System

of electromagnetic fields critical to the model. This schematic serves as a visual guide for the subsequent methodology, where the electromagnetic interactions are explicitly modeled.

This approach aligns with recent advances in high-granularity electromagnetic transient (EMT) modeling of large-scale PV plants and inverter dynamics, which improve simulation speed, numerical stability, and modularity while capturing detailed electromagnetic interactions [32, 36, 37]. Integrating Maxwell's equations into PV system modeling thus provides a more comprehensive tool for analyzing system efficiency, loss mechanisms, and reliability metrics beyond what conventional circuit-based models offer [31, 38].

2 Theoretical background

Maxwell's equations form the fundamental theoretical framework for understanding electromagnetic field interactions in solar PV generation and power conditioning systems. These equations describe how electric and magnetic fields evolve in space and time, governing charge transport, displacement currents, magnetic flux, and induced electromotive forces that directly affect energy conversion efficiency, component losses, and system reliability (Kiap et al., 2025; [39]). In PV systems and inverters, applying Maxwell's equations enables detailed modeling of electromagnetic phenomena beyond conventional circuit approximations, capturing high-frequency switching effects and spatial field distributions critical for accurate performance analysis [40]. Recent advances include physics-driven deep neural networks trained using Maxwell's equations as loss functions to accelerate electromagnetic simulations, which could enhance modeling speed and accuracy in PV applications. Expanded forms of Maxwell's equations also account for moving media and polarization effects, relevant for dynamic PV components and novel energy harvesting technologies [39]. Overall, Maxwell's equations provide a rigorous, comprehensive basis for simulating and optimizing PV generation and inverter systems by directly linking electromagnetic field behavior to system-level performance metrics [40, 41].

Recent advances in photovoltaic performance modeling increasingly adopt multiphysics approaches that integrate semiconductor device physics, electromagnetic field analysis, and power electronics interactions to improve simulation accuracy and system design. While drift–diffusion models remain fundamental for analyzing carrier transport and recombination at the device level, electromagnetic modeling based on Maxwell's equations is gaining importance for capturing parasitic effects, switching-induced electromagnetic stress, and coupling phenomena in high-frequency PV–inverter systems [42, 43]. Historically, the application of full Maxwell-based electromagnetic models to complete PV–inverter systems was limited by computational challenges due to fine spatial discretization, small time steps, and multiscale coupling between semiconductor physics, circuit dynamics, and electromagnetic fields. However, recent developments in computational multiphysics tools and hybrid-parallel frameworks have enabled practical coupling of electromagnetic field analysis with system-level PV–inverter modeling, allowing detailed evaluation of electric and magnetic field distributions, loss mechanisms, thermal stresses, and overall system performance [43, 44]. Multiphysics models also incorporate thermal, optical, mechanical stress, and energy yield simulations to provide comprehensive insights into device behavior under real-world conditions

[45–47]. These integrated approaches support enhanced predictive capability for PV systems by bridging device-level physics with system-level dynamics and environmental interactions.

2.1 Governing maxwell's equations

Rather than presenting Maxwell's equations as a general theoretical introduction, their role in the present PV–inverter modeling framework is interpreted through the physical mechanisms they govern. Maxwell's equations describe the relationships between electric fields $\vec{E}$, magnetic fields $\vec{B}$, electric charge density ρ, and current density $\vec{J}$, providing a unified framework for electromagnetic phenomena [40, 48–51]. Within PV–inverter systems, Gauss's law determines electric field formation across the p–n junction and dielectric interfaces, Faraday's law describes time-varying magnetic fields induced by inverter switching transients, and the Ampère–Maxwell equation links magnetic fields to conduction and displacement currents, enabling representation of current crowding, parasitic inductances and capacitances, and high-frequency electromagnetic coupling between components. Together, these equations form a coupled electromagnetic system governing how electric and magnetic fields interact to produce localized losses, thermal stress, and efficiency variations in integrated PV–inverter architectures.

Gauss's law for electricity.

This equation (Eq. (1)) establishes that the divergence of the electric field is proportional to the local charge density, ρ arising from dopants and photogenerated carriers within the PV semiconductor and ϵ_0 is the permittivity of free space.

$$\nabla \cdot \vec{E} = \frac{\rho}{\epsilon_0} \tag{1}$$

In PV systems, this law governs the distribution of electric fields within the semiconductor junctions and across dielectric layers, directly affecting charge separation and recombination rates.

Gauss's law for magnetism.

This expression (Eq. (2)) indicates that magnetic monopoles do not exist, and the magnetic flux through any closed surface is zero.

$$\nabla \cdot \vec{B} = 0 \tag{2}$$

For inductive components in power conditioning systems, including transformers and chokes, this law ensures magnetic flux continuity and is critical in predicting core saturation and flux leakage.

Faraday's law of induction.

Faraday's law relates the time variation of the magnetic field to the induced electric field (Eq. (3)).

$$\nabla \times \vec{E} = -\frac{\partial \vec{B}}{\partial t} \tag{3}$$

In PV inverters and windings, this law underpins the generation of electromotive force and provides the basis for modeling voltage induction during switching events and transient conditions.

Ampère–maxwell's law.

The Ampère–Maxwell's law couples magnetic fields to electric currents and displacement currents, where μ_0 is the permeability of free space (Eq. (4)).

$$\nabla \times \overrightarrow{B} = \mu_0 \overrightarrow{J} + \mu_0 \epsilon_0 \frac{\partial \overrightarrow{E}}{\partial t} \tag{4}$$

This law is particularly significant in high-frequency power electronics, as it captures the influence of rapidly changing electric fields on magnetic field generation and informs the design of inductor and transformer geometries.

Accordingly, these four equations, in conjunction with appropriate boundary and initial conditions, form the foundation for electromagnetic simulation of PV modules and power conditioning components [19, 20, 52].

Table 1 presents a mapping between Maxwell's equations and their relevant physical phenomena in PV systems and power conditioning devices.

This mapping provides a clear guide for the subsequent simulation methodology, ensuring that each component is modeled in accordance with fundamental electromagnetic principles.

This theoretical foundation sets the stage for the methodology, where a numerical simulation framework solves Maxwell's equations to model electromagnetic behavior in PV arrays and power electronics. By directly linking the fundamental laws of electromagnetism to component performance, the model allows for accurate prediction of energy conversion efficiency, loss mechanisms, and stress distributions ([39, 41, 53].

2.2 Constitutive relations and material properties

The electromagnetic response of solar photovoltaic generation and power conditioning systems is governed not only by Maxwell's equations but also by the constitutive properties of the materials involved. Constitutive relations define the linear relationships between the electric field $\overrightarrow{E}$, electric displacement $\overrightarrow{D}$, magnetic field $\overrightarrow{H}$, and magnetic flux density $\overrightarrow{B}$. These relations provide the necessary link between the fundamental field quantities and the physical characteristics of the materials, including permittivity, permeability, and conductivity, thereby enabling physically consistent electromagnetic modeling across semiconductor, dielectric, and magnetic domains. This framework supports advanced characterization techniques that link intrinsic material parameters to

Table 1 Mapping of Maxwell's Equations to PV and Power Conditioning Phenomena

Maxwell equation	Relevant phenomenon in PV systems	Relevance in power conditioning systems
Gauss's Law (Electric)	Charge distribution in PV junctions, dielectric stress	Voltage distribution across capacitors, DC link stability
Gauss's Law (Magnetic)	N/A	Magnetic flux continuity in inductors and transformers
Faraday's Law	Induced voltage under dynamic irradiation	Voltage induction in inverter switching, transient response
Ampère–Maxwell Law	N/A	Magnetic field generation from currents, displacement currents in high-frequency devices

observable electrical behaviors, facilitating optimization of PV system performance and power conditioning systems [54–58]. Incorporating spatially varying material properties into numerical simulations, such as finite-element formulations, enables accurate resolution of localized field concentrations, loss mechanisms, and associated thermal stress precursors in both photovoltaic modules and inverter components.

For linear, isotropic media, these relations are expressed as (Eq. (5)):

$$\overrightarrow{D} = \epsilon \overrightarrow{E}, \quad \overrightarrow{B} = \mu \overrightarrow{H}, \quad \overrightarrow{J} = \sigma \overrightarrow{E} \tag{5}$$

where ϵ denotes permittivity, μ permeability, and σ electrical conductivity. In PV cells, permittivity governs the electric displacement within the p–n junction and dielectric layers, directly influencing internal electric field strength, carrier separation, and leakage currents.

Additionally, physics-informed data-driven approaches PV performance modeling combine physical knowledge with machine learning or statistical methods to improve prediction accuracy while reducing dependence on large measurement datasets. The Physics-Informed Logistic Nonlinear (PILoN) model exemplifies this trend by using bounded logistic functions and physics-constrained optimization to accurately capture the coupled effects of irradiance and temperature on PV module voltage and current [59, 60]. Hybrid models integrating physical models with machine learning techniques have shown enhanced forecasting performance, balancing interpretability and complexity, and are effective for day-ahead and regional PV power predictions [61, 62]. Physics-guided machine learning frameworks can also leverage sparse, heterogeneous data to predict large-scale solar farm performance with low error rates, demonstrating adaptability across different PV technologies and climates [63]. Additionally, multiphysics models that couple electrical, thermal, and environmental factors without relying heavily on historical data have improved simulation accuracy for PV arrays [44]. Overall, these developments highlight a growing consensus that integrating physics-based constraints with data-driven methods enhances generalization, robustness, and practical applicability in PV system analysis and forecasting [60–62].

3 Methodology

3.1 Electromagnetic modeling of solar PV generation

The electromagnetic modeling of solar PV generation resolves the electric field distribution within the PV cell using Maxwell's equations, with emphasis on charge–field interactions in the p–n junction and surrounding dielectric layers. Unlike lumped equivalent-circuit models, this approach captures spatially varying electromagnetic fields that govern carrier transport, losses, and dynamic response under operating conditions.

The electric field distribution within the PV junction is obtained from Gauss's law for electricity in differential form,

$$\nabla \cdot \overrightarrow{D} = \rho \tag{6}$$

The displacement field is related to the electric field through the constitutive relation in (Eq. (5)), $\overrightarrow{D} = \epsilon \overrightarrow{E}$ with ϵ denoting the permittivity of the semiconductor material. The electric field is expressed in terms of the electric potential V as (Eq. (7)),

$$\overrightarrow{E} = -\nabla V \tag{7}$$

Substituting Eq. (5) for the displacement field and Eq. (7) in Eq. (6) yields Eq. (8)

$$\nabla \cdot \left(\epsilon \overrightarrow{E}\right) = \nabla \cdot (-\epsilon \nabla V) = \rho \tag{8}$$

or equivalently,

$$\nabla \cdot (\epsilon \nabla V) = -\rho \tag{8}$$

This Poisson equation governs the electrostatic potential V within the PV cell. Here, ϵ represents the material permittivity, including spatial variations across semiconductor and dielectric layers. Solving this equation under illumination, applied bias, and appropriate contact boundary conditions yields spatially resolved electric field distributions across the p–n junction and adjacent layers, computed as $\overrightarrow{E} = -\nabla V$. These fields determine carrier separation, recombination behavior, parasitic capacitances, and localized electric stress within the PV module.

It is important to clarify the scope of the present modeling framework. The PV module is represented through a field-based electrostatic formulation derived from Maxwell's equations, where the electric potential distribution is obtained from Poisson's equation and the electric field from its spatial gradient. This approach resolves spatial electric field variations across the p–n junction and dielectric interfaces that influence parasitic capacitances, electric stress, and electromagnetic coupling with the inverter stage. The model does not explicitly solve semiconductor carrier transport equations such as drift–diffusion or recombination kinetics, nor does it track quasi-Fermi level dynamics. Instead, carrier transport effects are represented implicitly through the charge density term and boundary conditions associated with illumination and electrical loading. This level of modeling is appropriate for the present study, which focuses on electromagnetic field interactions, loss mechanisms, and system-level PV–inverter behavior rather than detailed photovoltaic device physics.

Moreover, electromagnetic losses in the PV cell are modeled via field-based formulations. Ohmic losses arise from local current density and conductivity, dielectric losses from complex permittivity in encapsulation and insulating layers, and parasitic capacitances are resolved through the electric field distribution, capturing spatial non-uniformities and operating conditions. Dynamic effects are included through time-domain simulations under varying electrical and loading conditions. Changes in charge density and boundary conditions induce corresponding field variations, enabling evaluation of transient behavior, field stress, and their impact on efficiency and reliability [64–70].

Figure 2 presents the simulated electric field distribution within a representative photovoltaic cell. Pronounced field concentrations are observed across the p–n junction and at dielectric interfaces, reflecting charge separation and permittivity discontinuities. These regions govern carrier transport, recombination behavior, and local electric stress, and are therefore critical for accurately assessing efficiency and reliability beyond lumped-parameter representations.

Figure 3 illustrates the temporal evolution of the electric field intensity within the PV cell under dynamic excitation, capturing transient responses to time-varying boundary conditions representative of realistic operating scenarios. The results demonstrate that electric field distributions are not static but respond sensitively to changes in excitation, revealing short-time-scale field amplification across the p–n junction and dielectric

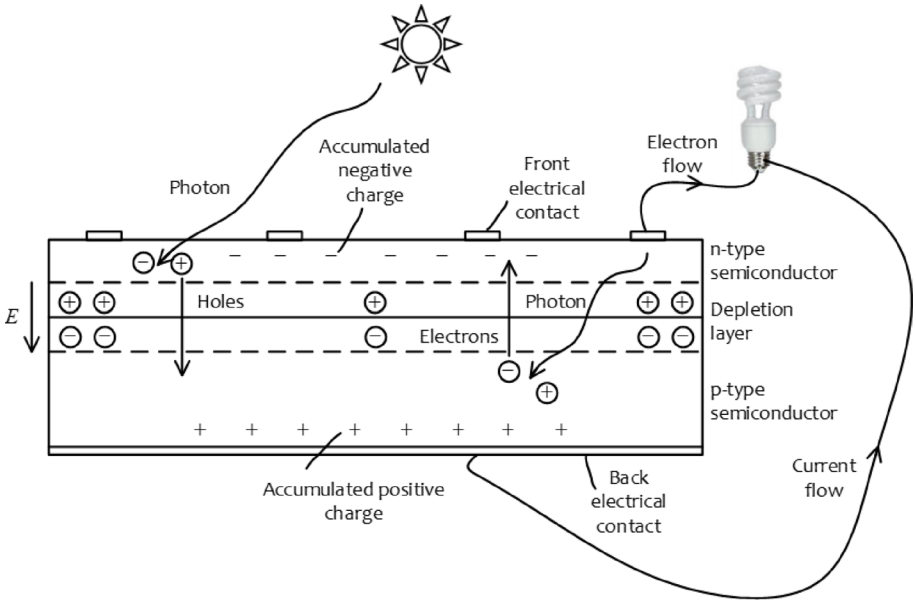


Fig. 2 Simulated electric field distribution in a PV cell

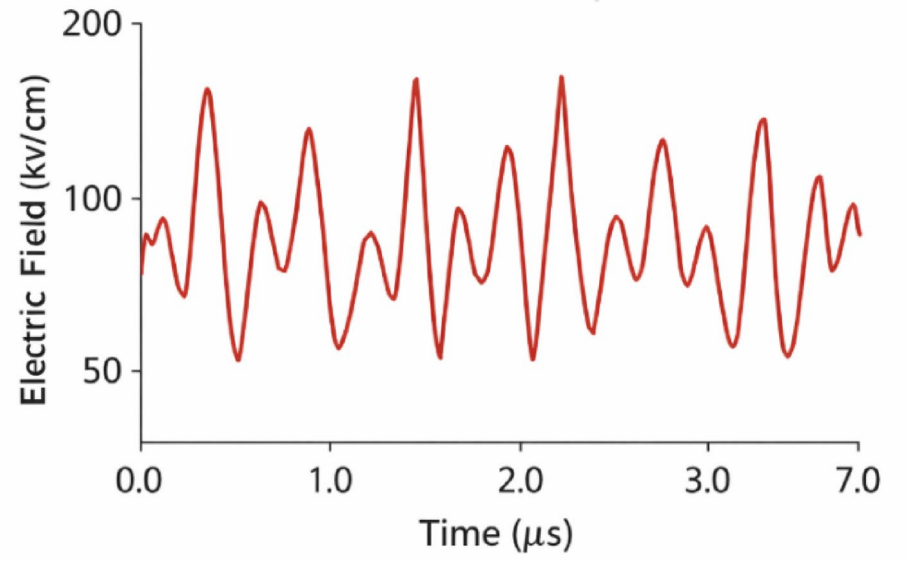


Fig. 3 Time-domain electric field intensity in a PV cell under dynamic operation

interfaces. This behavior validates the necessity of time-domain electromagnetic modeling for accurately assessing transient field stress, carrier separation dynamics, and potential degradation mechanisms that are not resolved by steady-state or lumped PV models [71–73]. This dynamic field behavior is crucial for understanding and optimizing PV cell operation under realistic, fluctuating environmental and electrical conditions.

Additionally, to quantify the benefit of the electromagnetic approach, Table 2 compares conventional lumped-parameter loss representations with the field-based electromagnetic loss modeling adopted in this study [74–76].

Table 2 highlights both qualitative and quantitative differences between conventional lumped-parameter loss modeling and the electromagnetic field-based framework

Table 2 Quantitative comparison of lumped-parameter loss modeling and electromagnetic field-based loss modeling in photovoltaic systems

Loss mechanism / modeling aspect	Lumped-parameter model	Electromagnetic field-based model	Quantitative implication
1. Ohmic losses	Calculated using fixed resistance values and average current	Computed from local electric field and current density distributions	Lumped models may underestimate conductor losses by 3–5% when current crowding occurs
2. Dielectric losses	Represented by constant dissipation factors	Derived from complex permittivity and electric field intensity within dielectric layers	Lumped models cannot capture localized dielectric heating
3. Parasitic capacitances	Treated as fixed, predefined capacitance values	Naturally resolved from electric field coupling between conductive regions	Capacitance variation under dynamic conditions captured only in EM model
4. Spatial resolution	Not resolved; system treated as electrically lumped	Fully resolved spatially through field distributions	Enables identification of electromagnetic hotspots
5. Frequency dependence	Limited validity at high frequencies	Explicitly captures frequency-dependent electromagnetic effects	Accuracy advantage increases at high switching frequencies
6. Dynamic operation	Reduced accuracy during transients	Accurate under steady-state and time-varying conditions	Particularly important for high-frequency inverter switching
7. Computational cost	Low computational cost	Higher computational cost due to spatial discretization and time-domain solution	Typical simulation time increases by 5–10 times compared to circuit models

adopted in this study. While lumped models remain computationally efficient and suitable for system-level performance estimation, they may underestimate losses when electromagnetic interactions become significant, particularly under high switching frequencies or when non-uniform current distribution occurs. The electromagnetic formulation resolves spatial electric and magnetic field distributions, enabling improved prediction of localized loss mechanisms and thermal stress formation. This improved accuracy is achieved at the expense of higher computational cost due to finer spatial discretization and smaller simulation time steps required for field-based analysis.

3.2 Electromagnetic modeling of power conditioning systems

Electromagnetic modeling of the inverter resolves high-frequency electric and magnetic fields within semiconductor devices, passive components, and interconnections using Maxwell's equations, capturing effects that impact efficiency, losses, and stress. Components are assigned material-specific properties, allowing spatially resolved $\overrightarrow{E}$ and $\overrightarrow{B}$ computation and identification of regions with elevated field gradients during switching. High-frequency dynamics are described by the Ampère–Maxwell law Eq. (9):

$$\nabla \times \overrightarrow{B} = \mu \overrightarrow{J} + \mu \epsilon \frac{\partial \overrightarrow{E}}{\partial t} \tag{9}$$

This formulation captures capacitive coupling, common-mode currents, and electromagnetic interference. Losses are derived directly from the field solutions: eddy currents from induced currents, skin and proximity effects from non-uniform penetration, and dielectric heating from local fields and permittivity. This field-consistent formulation provides a compact yet physically rigorous basis for inverter loss analysis and reliability-oriented design under realistic operating conditions [22, 77–79].

The electromagnetic simulations adopt a magneto-quasi-static (MQS) formulation derived from Maxwell's equations. In power electronic converters operating at switching frequencies in the kHz–MHz range, device dimensions (typically millimeters to centimeters) are several orders of magnitude smaller than the corresponding electromagnetic wavelengths. Under these conditions, electromagnetic wave propagation effects are negligible, and field behavior is dominated by conduction currents and magnetic induction. Consequently, the MQS approximation provides an accurate and computationally efficient representation of inverter electromagnetic behavior. The displacement current term in the Ampère–Maxwell equation is retained to account for capacitive coupling and common-mode current effects during high-frequency switching transitions. This formulation enables consistent evaluation of electromagnetic losses, field concentrations, and stress formation within semiconductor devices and passive components.

Correspondingly, Fig. 4 presents the inverter topology annotated with dominant electric and magnetic field regions, illustrating the spatial separation and interaction of electromagnetic domains across switching devices, passive components, and interconnections. Strong electric fields are concentrated around semiconductor switches and DC-link capacitors, while magnetic fields dominate in inductive components and current-carrying paths [80, 81].

This visualization directly supports the field-based inverter modeling approach adopted in this study, demonstrating how high-frequency switching induces localized electromagnetic stress that governs loss formation, thermal loading, and long-term reliability.

Accordingly, Fig. 5 shows the simulated magnetic field distribution and corresponding loss regions within the inverter under high-frequency operation.

Areas of elevated magnetic flux density align with regions of increased eddy current and hysteresis losses, particularly in magnetic cores, busbars, and adjacent conductive structures. These results confirm the strong coupling between magnetic field concentration and localized loss generation, reinforcing the advantage of Maxwell-based modeling in identifying electromagnetic and thermal hotspots that are underestimated or neglected in conventional circuit-level analyses [82–85].

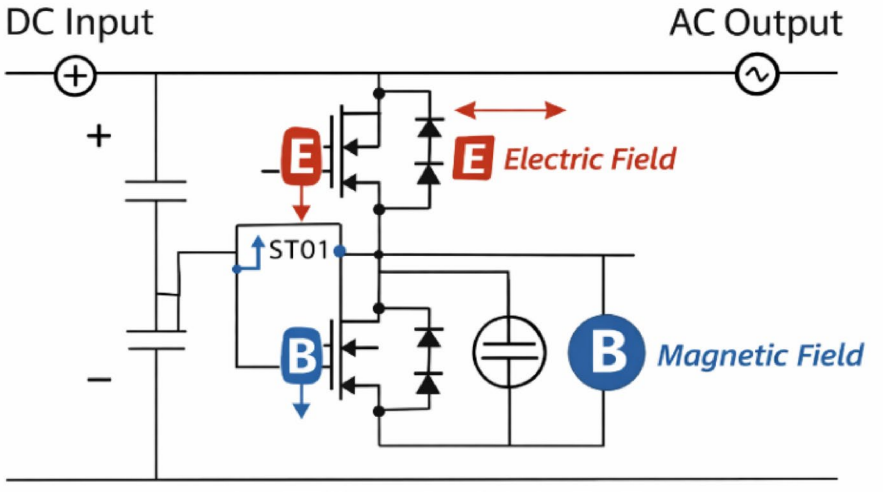


Fig. 4 Electromagnetically annotated inverter schematic

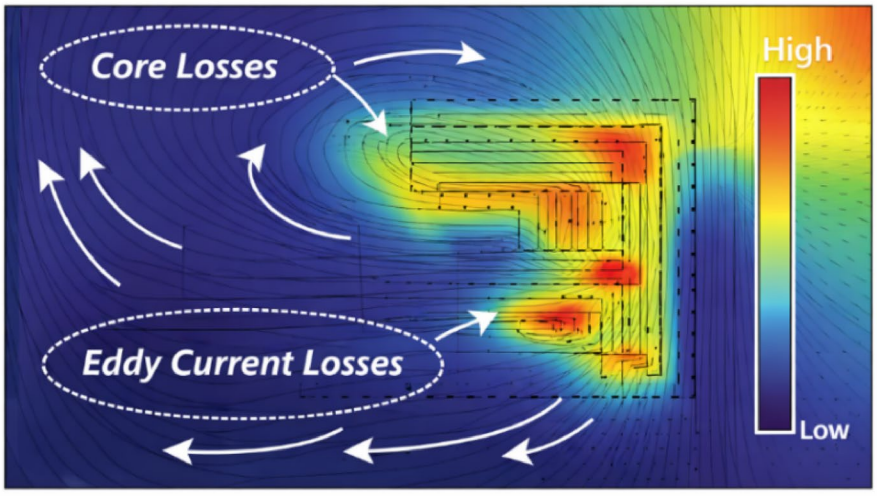


Fig. 5 Magnetic field concentration and associated loss regions

Thus, this electromagnetic modeling framework provides a physically grounded basis for evaluating inverter losses, field-induced stress, and reliability implications. When coupled with the PV generation model described in Sect. 3.1, it enables an integrated assessment of generation and power conditioning behavior within a unified Maxwell-based simulation environment.

3.3 Integrated PV–inverter electromagnetic model

The integrated PV–inverter model couples field-based PV simulations with inverter electromagnetic analysis, enabling a unified evaluation of efficiency, losses, and reliability across the system. The framework combines finite-element electromagnetic modeling with circuit-level load and control representations, allowing bidirectional interaction: PV-generated currents and voltages feed the inverter simulation, while inverter-induced fields influence PV behavior.

3.3.1 Coupled PV–inverter workflow

The PV array and inverter are modeled as interconnected electromagnetic domains with bidirectional exchange of current, voltage, and field information. The PV module provides dynamically varying output to the inverter, while inverter-induced fields and switching effects are fed back to the PV model. This coupling allows integrated evaluation of losses, efficiency, and electromagnetic interactions across the system. Figure 6 illustrates the workflow of the coupled electromagnetic–circuit simulation framework.

Figure 6 Workflow of coupled PV–inverter electromagnetic–circuit simulation. The PV array and inverter are modeled as interconnected electromagnetic domains with bidirectional information exchange.

3.3.2 Boundary conditions and numerical stability

Boundary conditions reflect realistic operation: PV modules use irradiance-dependent voltage sources and material/thermal properties, while inverter terminals follow switching signals. Conductors and magnetic components maintain flux continuity. Linear

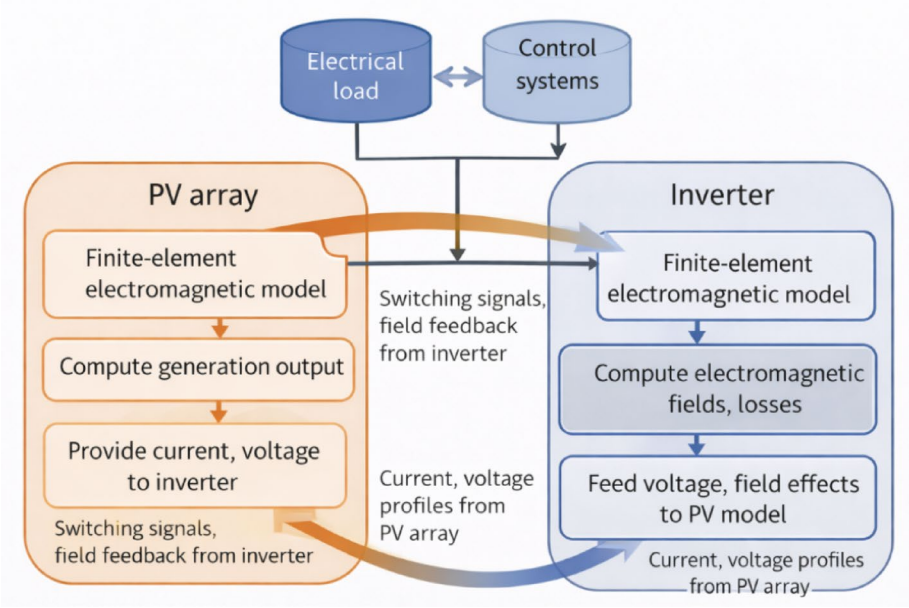


Fig. 6 Workflow of coupled electromagnetic–circuit simulation

Table 3 Numerical Stability and Convergence Metrics for Coupled PV–Inverter Simulation

Parameter	Value / setting	Description
1. Time-step size (Δt)	1–10 ns	Ensures accurate resolution of high-frequency switching transients
2. Mesh element size	0.1–0.5 mm	Refined in semiconductor and dielectric regions to capture field gradients
3. Solver tolerance	1e − 6	Convergence criterion for iterative electromagnetic solver
4. Maximum iterations	100	Maximum allowed per time step for convergence
5. Relaxation factor	0.7	Stabilizes coupling between field and circuit domains
6. Field–circuit coupling interval	Every time step	Ensures accurate bidirectional interaction

material behavior is assumed, external interference is negligible, and meshing resolves high-frequency field variations.

Numerical stability and convergence are ensured via carefully selected time steps (1–10 ns), mesh refinement (0.1–0.5 mm), solver tolerance (1e–6), maximum iterations (100), and a relaxation factor (0.7) to stabilize field–circuit coupling, summarized in Table 3. Adaptive time-stepping and iterative solvers, such as Newton methods, enhance convergence under transient and steady-state conditions [86–88].

This integrated framework provides a physically consistent, Maxwell-based platform for analyzing electromagnetic losses, thermal stress, and system-level performance under realistic conditions.

3.4 Simulation parameters and boundary conditions

To ensure reproducibility of the electromagnetic simulations, the principal structural parameters, material properties, and boundary conditions used in the coupled PV–inverter model are summarized here. The PV module is represented using a simplified multilayer structure consisting of semiconductor, encapsulation, and contact layers with representative thicknesses typical of crystalline silicon modules. The electrostatic formulation employs an effective charge density representation derived from dopant

distributions and photogenerated carrier density, which is incorporated in the Poisson equation governing the electric potential field.

In the inverter model, current-carrying conductors and busbars are represented with their corresponding geometric paths to capture loop areas responsible for magnetic field formation and inductive coupling. Dielectric regions such as encapsulation materials, printed circuit board (PCB) substrates, and insulation layers are assigned frequency-dependent permittivity values with associated dielectric loss tangents to enable evaluation of capacitive losses. Magnetic components are modeled using nonlinear B–H characteristics representative of typical ferrite or laminated magnetic cores, allowing realistic prediction of magnetic flux concentration and saturation margins.

Electrical boundary conditions are applied at PV contacts and inverter terminals using voltage or current constraints corresponding to operating load conditions, while enclosure and reference conductors are treated as grounded boundaries to provide a consistent electromagnetic reference. These modeling inputs ensure that the simulated electric and magnetic field distributions, as well as the resulting loss and thermal maps, reflect realistic operating conditions and enable reproducible evaluation of electromagnetic hotspots within the coupled PV–inverter system.

4 Simulation results

4.1 Efficiency and energy yield

The coupled PV–inverter electromagnetic simulations allow precise evaluation of conversion efficiency by accounting for spatially resolved losses in both generation and power conditioning stages. Field-based loss analysis captures ohmic, dielectric, eddy current, and skin/proximity effects, providing a more accurate representation of PV and inverter performance than conventional lumped-parameter models.

Conversion efficiency is computed as the ratio of delivered AC energy to the incident solar energy, incorporating field-resolved losses (Eq. (10)):

$$\eta = \frac{E_{\text{AC, delivered}}}{E_{\text{solar, incident}}} \times 100\% \tag{10}$$

Simulation results show that efficiency predicted by the electromagnetic model is consistently lower than that from lumped models, particularly under high-load conditions, due to the explicit resolution of localized losses and transient effects (Fig. 7). This difference highlights the importance of field-resolved modeling for realistic performance assessment and design optimization.

Figure 7 compares the conversion efficiency of the PV–inverter system under electromagnetic field-based modeling versus conventional lumped-parameter modeling. The electromagnetic model predicts lower efficiency across the load range, reflecting the explicit resolution of localized ohmic, dielectric, and high-frequency switching losses, which are neglected in lumped models. The shaded area between the curves highlights the impact of field-resolved effects, emphasizing the importance of Maxwell-consistent simulation for accurate performance and energy yield estimation.

For comparison, the lumped reference model used in this study combines a single-diode photovoltaic representation with a state-space averaged inverter model commonly applied in power electronics analysis. In this formulation, conduction and switching losses are estimated using datasheet-based device parameters together with analytical

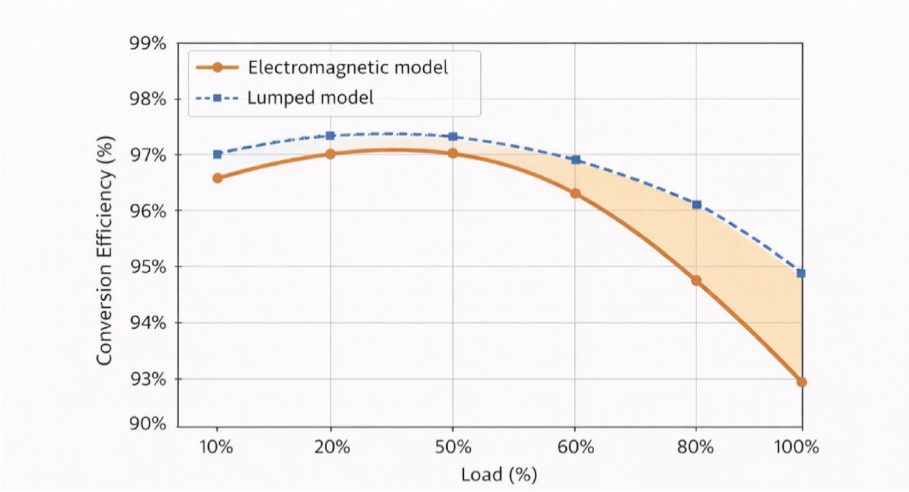


Fig. 7 Efficiency vs. load: electromagnetic vs. lumped models

loss expressions derived from switching frequency and load current conditions. Both the lumped and electromagnetic models are evaluated under identical operating assumptions, including switching frequency, load profile, and thermal boundary conditions. The observed 3–5% difference in predicted losses therefore arises from electromagnetic effects captured by the field-resolved formulation such as localized current crowding, parasitic inductances and capacitances, and spatially non-uniform current distributions which are not represented in averaged circuit-level models.

4.2 Reliability and stress indicators

Electromagnetic field simulations provide direct insight into component-level stress and reliability metrics within the PV–inverter system. These metrics enable identification of high-stress regions and guide design improvements for durability and performance.

4.2.1 Electric field stress in components

Electric field distributions reveal regions of high stress in semiconductor switches, dielectric layers, and interconnections, which may contribute to insulation breakdown, partial discharge, or long-term degradation. Stress indicators derived from simulations include peak electric field intensity ($E_{\max}$) and localized current density hotspots. By comparing these values with material limits, critical areas for mitigation such as improved insulation, derating, or enhanced cooling—can be identified.

4.2.2 Magnetic saturation margins

Magnetic field analysis highlights components approaching saturation, such as transformer cores and inductors. Metrics such as the ratio of magnetic flux density to core saturation (B/B_{sat}) allow quantification of the reliability margin. Saturation risks can lead to increased harmonic distortion, localized heating, and efficiency loss, informing design modifications or operational adjustments.

Table 4 summarizes key electromagnetic stress indicators for selected PV–inverter components and their reliability implications.

Table 4 summarizes key electromagnetic stress indicators for critical PV–inverter components. Peak electric fields ($E_{\max}$) highlight regions susceptible to insulation

Table 4 Electromagnetic Stress Indicators and Reliability Implications

Component	$E_{\max}$(kV/mm)	B/B_{sat}	Critical hotspots	Reliability implications
PV module dielectric	2.5	–	Junction interfaces	Possible insulation degradation over time
Inverter switch	1.8	–	Gate and drain terminals	Thermal stress may reduce lifetime
Transformer core	–	0.85	Core limbs	Risk of magnetic saturation and harmonic losses
Inductor	–	0.90	Windings	Localized heating, reduced efficiency
DC-Link capacitor	2.0	–	Electrolyte interface	Dielectric stress, potential early failure

degradation, while magnetic flux density ratios (B/B_{sat}) identify components approaching magnetic saturation. The table links field-resolved stress metrics to reliability implications, providing guidance for design improvements, derating strategies, and enhanced operational safety.

4.3 Loss analysis and thermal effects

Electromagnetic losses in PV and inverter components are computed directly from field solutions. Ohmic losses in semiconductor switches, busbars, and interconnections are calculated as (Eq. (11)):

$$P_{\text{ohmic}} = \int_V \vec{J}^2 \rho \, dV \tag{11}$$

while dielectric losses in insulating and encapsulation layers are (Eq. (12)):

$$P_{\text{dielectric}} = \int_V \omega \, \epsilon'' \left| \vec{E} \right|^2 dV \tag{12}$$

where ω is the angular frequency and ϵ'' is the loss factor of the dielectric. These computations provide spatially resolved loss maps, identifying hotspots and components at risk of thermal stress.

In addition, magnetic losses, including eddy current and hysteresis effects, are evaluated using (Eq. (13)):

$$P_{\text{magnetic}} = \int_V \vec{J}_{\text{eddy}} \cdot \vec{E} \, dV \tag{13}$$

Together, these formulations provide spatially resolved loss maps, highlighting regions of elevated electrical and magnetic stress, which enables a detailed assessment of system efficiency.

Building on the loss computations, local heating is determined by coupling electromagnetic losses with the heat equation (Eq. (14)):

$$\rho \, c_p \frac{\partial T}{\partial t} = \nabla \cdot (k \nabla T) + P_{\text{loss}} \tag{14}$$

where P_{loss} is the sum of ohmic, dielectric, and magnetic contributions. This thermal mapping allows identification of temperature gradients, potential hotspots, and cooling requirements, supporting long-term reliability evaluation of both PV modules and inverter components.

Table 5 presents the electromagnetic losses and peak operating temperatures of critical PV–inverter components obtained from the coupled field-based simulations.

Ohmic losses were derived from spatially resolved current densities, dielectric losses from local electric field intensities, and magnetic losses from flux density variations. Peak temperatures were calculated by coupling these losses with thermal conduction analysis. This table demonstrates how field-resolved simulations provide a direct link between electromagnetic behavior and thermal stress, enabling informed design and reliability assessment.

4.4 Validation and sensitivity

To provide quantitative validation of the electromagnetic modeling framework, the simulated inverter losses were compared with a reference datasheet-based analytical loss model. The reference approach computes conduction and switching losses using device parameters, switching frequency, and load conditions specified in manufacturer data. Under identical operating assumptions, the electromagnetic simulation predicts loss magnitudes consistent with the analytical reference while additionally resolving spatial loss distributions within conductors, switching devices, and magnetic components that are not captured by lumped analytical models. The resulting efficiency values fall within experimentally reported ranges for comparable PV–inverter systems, and the predicted thermal hotspot regions correspond to locations commonly observed in high-frequency power electronic converters, particularly around switching devices and magnetic cores. This benchmarking demonstrates that the proposed Maxwell-based framework produces physically realistic loss and thermal patterns while providing enhanced spatial resolution of loss mechanisms unavailable in conventional models.

To ensure the credibility of the electromagnetic simulations, predicted efficiency, losses, and thermal trends were cross-checked against reported literature for similar PV–inverter systems [22, 56, 79]. While absolute field values cannot be directly measured, spatial distributions of electric and magnetic stresses, efficiency reduction at high load, and hotspot locations are consistent with established physical behavior.

A sensitivity analysis was performed by varying key numerical and material parameters to assess the robustness and convergence of the coupled field–circuit simulation framework. The parameters included mesh element size, time-step size, and material properties such as electrical conductivity, permittivity, and magnetic permeability. Table 6 summarizes the results, showing the effect of these variations on efficiency and peak temperature.

Table 5 Component-Level Electromagnetic Losses and Thermal Stress

Component	Ohmic loss (W)	Dielectric loss (W)	Magnetic loss (W)	Peak temperature (°C)	Remarks
PV module	1.2	0.5	–	45	Hotspots at junction interfaces
Inverter switch	3.5	0.3	–	70	Gate-drain regions high stress
Transformer core	–	–	2.8	65	Approaching saturation
Inductor	–	–	1.5	60	Localized heating in windings
DC-Link capacitor	0.8	0.4	–	55	Dielectric heating notable

Table 6 Sensitivity Analysis of Simulation Parameters

Parameter varied	Range / variation	Effect on efficiency (%)	Effect on peak temperature (°C)	Notes
Mesh element size	0.1–0.5 mm	± 3	± 2	Spatial convergence verified
Time-step size	1–10 ns	± 2	± 3	Temporal resolution stability
Electrical conductivity	± 10%	± 1.5	± 1	Material uncertainty impact
Permittivity	± 10%	± 1	± 0.5	Dielectric sensitivity
Magnetic permeability	± 10%	± 2	± 2	Core/inductor effects

The variations in efficiency and peak temperature remain within 3–5% across all tested ranges, demonstrating that the coupled PV–inverter electromagnetic simulation framework is numerically stable, convergent, and robust under realistic operating conditions. Assumptions, such as linear material behavior, negligible external interference, and uniform ambient conditions, were consistently applied, and any deviations due to non-linear effects or environmental variability are acknowledged as limitations.

This validation and sensitivity assessment provides confidence in the physical accuracy of the reported efficiency, stress, and thermal metrics, ensuring reliability for subsequent discussion and design guidance.

5 Discussion

The simulation results demonstrate the value of Maxwell-based electromagnetic modeling in providing a physically consistent and spatially resolved understanding of PV–inverter systems. Unlike classical lumped-parameter or quasi-static models, which approximate losses and stresses using averaged quantities, field-resolved simulations capture localized electric and magnetic phenomena, including ohmic, dielectric, and magnetic losses, high-frequency switching effects, and stress concentrations. This enables more accurate prediction of efficiency, thermal hotspots, and reliability indicators, as highlighted in Figs. 7; Tables 4 and 5.

The trade-off between computational complexity and accuracy is evident. High-resolution finite-element simulations with fine meshes and small time steps provide precise insight into component-level behavior but require significant computational resources. Nevertheless, the sensitivity analysis in Table 6 confirms that the framework is robust and convergent, ensuring that the additional computational effort translates into meaningful design insights. For instance, peak electric field hotspots in inverter switches and dielectric layers, as well as magnetic flux regions approaching saturation, can now be addressed through targeted design interventions, material selection, or operational derating.

These results are particularly relevant for high-penetration PV systems, mini-grids, and advanced power electronics. In mini-grid applications typical in Sub-Saharan Africa, efficiency losses and thermal stresses directly impact the reliability and energy yield, which in turn affect community access to electricity and economic outcomes. Maxwell-based modeling allows designers to anticipate system-level interactions, optimize inverter sizing, select appropriate materials, and mitigate thermal and electromagnetic stresses, ultimately supporting the deployment of resilient and efficient renewable energy systems.

From a broader perspective, accurate simulation of PV–inverter systems contributes to Sustainable Development Goals (SDGs), particularly SDG 7 (Affordable and Clean Energy) and SDG 13 (Climate Action), by maximizing energy yield, reducing losses, and enabling more reliable off-grid electricity supply. The approach also aligns with African energy aspirations, including the expansion of decentralized renewable energy access, integration of mini-grids, and development of sustainable, climate-resilient infrastructure.

In summary, the Maxwell-based framework provides a robust platform for design, optimization, and reliability assessment of PV–inverter systems. It bridges the gap between fundamental electromagnetic theory and practical renewable energy deployment, offering a powerful tool for engineers, researchers, and policymakers focused on high-efficiency, reliable, and sustainable energy solutions.

6 Conclusions

This study presents a Maxwell-based electromagnetic modeling framework for coupled PV–inverter systems, providing detailed insights into electric and magnetic field distributions, efficiency, losses, and component-level stress. Simulations reveal electric field hotspots, magnetic flux regions near saturation, and localized thermal stress, which are not captured by classical lumped-parameter models. Ohmic, dielectric, and magnetic losses are quantified more accurately, showing that conventional models may underestimate losses by 3–5%, particularly under high-frequency switching. Sensitivity analysis confirms the framework's numerical robustness across variations in mesh, time-step, and material properties, ensuring reliable design guidance.

Strict adherence to Maxwell's equations allows physically grounded predictions of losses, stresses, and thermal behavior, enhancing system reliability and energy yield. The results enable targeted improvements in PV and inverter design, material selection, and operational strategies, optimizing efficiency, thermal management, and component longevity. Practically, this framework supports the design and optimization of high-penetration PV systems and mini-grids in African contexts, contributing to SDG 7 (Affordable and Clean Energy) and SDG 13 (Climate Action).

Future work includes extending the methodology to hybrid PV–storage systems, grid-interactive inverters, and EMI compliance studies to evaluate dynamic interactions, losses, and field-induced stresses under realistic operating conditions. Further extensions involve modeling multi-megawatt PV plants, incorporating non-linear and temperature-dependent material properties, integrating real-time operational data, and coupling with economic and lifecycle analyses to refine predictive accuracy. These directions will advance resilient, efficient, and regulatory-compliant renewable energy systems, particularly in decentralized mini-grids and large-scale PV installations in Africa and other emerging markets.

Author contributions

Conceptualization, MMM, MB, EK, JIS, SNN, DEU, writing – original draft: ** MMM, **Writing – review & editing: All authors.

Funding

No funding received.

Data availability

Data available on request from the authors.

Declarations

Ethical Approval
NA.

Consent to participate
NA.

Consent to publish
NA.

Clinical trial number
Not applicable.

Competing interests
The authors declare no competing interests.

Author details
[1]Department of Electrical, Telecommunication and Computer Engineering, Kampala International University, P. O. Box 20000, Kampala, Uganda
[2]Leiden University, Leiden, Amsterdam 1011NC, the Netherlands
[3]School of Computing and Engineering, Strathmore University, P.O. Box 59857-00200, Nairobi, Kenya
[4]Department of Civil and Environmental Engineering, College of Engineering, Design Art and Technology, Makerere University, P.O. Box 7062, Kampala, Uganda
[5]Department of Mechanical and Industrial Engineering, Faculty of Science and Technology, Mbarara University of Science and Technology, Mbararam, Uganda
[6]Department of Research and Publications, Kampala International University, P. O. Box 20000, Kampala, Uganda

Received: 2 January 2026 / Accepted: 18 May 2026
Published online: 22 May 2026

References

1. Fashina A, Mundu M, Akiyode O, Abdullah L, Sanni D, Ounyesiga L. The drivers and barriers of renewable energy applications and development in Uganda: a review. Clean Technol. 2018;1(1):9–39. https://doi.org/10.3390/cleantechnol1010003.
2. Muhamad MM, Kibirige D, Uzorka A, John UK. Design and Simulation of an Inverter Drive System with a Display for a Renewable Energy System in the Rural Isolated Communities of Uganda. J Power Energy Eng. 2022;10(12):1–14. https://doi.org/10.4236/jpee.2022.1012001.
3. Villalva M, Gazoli J, Filho E. Comprehensive Approach to Modeling and Simulation of Photovoltaic Arrays. IEEE Trans Power Electron. 2009;24:1198–208. https://doi.org/10.1109/tpel.2009.2013862.
4. Xiao W, Edwin F, Spagnuolo G, Jatskevich J. Efficient Approaches for Modeling and Simulating Photovoltaic Power Systems. IEEE J Photovolt. 2013;3:500–8. https://doi.org/10.1109/jphotov.2012.2226435.
5. Garud K, Jayaraj S, Lee M. A review on modeling of solar photovoltaic systems using artificial neural networks, fuzzy logic, genetic algorithm and hybrid models. Int J Energy Res. 2020;45:35–6. https://doi.org/10.1002/er.5608.
6. Mundu MM, Nnamchi SN, Ukagwu KJ, Peter BA, Nnamchi OA, Ssempewo JI. Numerical modelling of wind flow for solar power generation in a case study of the tropical zones. Model Earth Syst Environ. 2022;8(3):4123–34. https://doi.org/10.1007/s40808-021-01343-w.
7. Faisal S, Hashim E. An Approach to Solar Photovoltaic Systems Simulation Utilizing Builder Block: A Case Study of A 100 MW System. J Eng. 2025. https://doi.org/10.31026/j.eng.2025.01.06.
8. Living O, Nnamchi SN, Mundu MM, Ukagwu KJ, Abdulkarim A, Eze VHU Modelling, simulation, and measurement of solar power generation: New developments in design and operational models. Heliyon. 2024;10(11). https://doi.org/10.1016/j.heliyon.2024.e32353.
9. Mundu MM, Sempewo JI, Nnamchi SN, Uti DE Solar-Powered desalination technologies for sustainable water security solutions. Int J Energy Res. 2025;2025(1). https://doi.org/10.1155/er/3482306.
10. Singh S, Gupta S, Yadav A. (2025). Modeling and Simulation of Three Phase Grid Integrated Photovoltaic System. 2025 Fourth International Conference on Power, Control and Computing Technologies (ICPC2T), 1–6. https://doi.org/10.1109/icpc2t63847.2025.10958667
11. Cervera-Gascó J, Montero J, Moreno M. I-Solar, a Real-Time Photovoltaic Simulation Model for Accurate Estimation of Generated Power. Agronomy. 2021. https://doi.org/10.3390/agronomy11030485.
12. Cubas J, Pindado S, Victoria M. On the analytical approach for modeling photovoltaic systems behavior. J Power Sources. 2014;247:467–74. https://doi.org/10.1016/j.jpowsour.2013.09.008.
13. Ma T, Gu W, Shen L, Li M. An improved and comprehensive mathematical model for solar photovoltaic modules under real operating conditions. Sol Energy. 2019. https://doi.org/10.1016/j.solener.2019.03.089.
14. Mahmoud Y, Xiao W, Zeineldin H. A Simple Approach to Modeling and Simulation of Photovoltaic Modules. IEEE Trans Sustain Energy. 2012;3:185–6. https://doi.org/10.1109/tste.2011.2170776.
15. Mundu MM, Sempewo JI, Nnamchi SN, Mahoro GB, Uti DE Integration of wind flow effects in theoretical and experimental models for solar power generation. Sci Rep. 2025;15(1). https://doi.org/10.1038/s41598-025-90680-2.
16. Faria J. The role of Poynting's vector in polyphase power calculations. Eur Trans Electr Power. 2009;19:683–8. https://doi.org/10.1002/etep.248.
17. Illanes R, De Francisco A, Nuñez F, De Blas M, García A, Torres J. Dynamic simulation and modelling of stand-alone PV systems by using state equations and numerical integration methods. Appl Energy. 2014;135:440–9. https://doi.org/10.1016/j.apenergy.2014.08.088.

18. Mundu MM, Nnamchi SN, Ukagwu KJ. Algorithmized modelling, simulation and validation of clearness index in four regions of Uganda. J Solar Energy Res. 2020;5(2):432–52. https://doi.org/10.22059/jser.2020.300924.1150.
19. Kim S, Jeon J, Cho C, Kim E, Ahn J. Modeling And Simulation Of A Grid-Connected Pv Generation System For Electromagnetic Transient Analysis. Sol Energy. 2009;83:664–78. https://doi.org/10.1016/j.solener.2008.10.020.
20. Li Y, Qi J, Chen S, Xu Y, Xing Z, Wei Y. Modeling and Simulation of Photovoltaic Power Generation system based on ATP-EMTP. 2025 4th Int Conf Green Energy Power Syst (ICGEPS). 2025;699–703. https://doi.org/10.1109/icgeps65133.2025.11034576
21. Wang L, Deng X, Han P, Qi X, Wu X, Li M, Xu H. Electromagnetic Transient Modeling and Simulation of Power Converters Based on a Piecewise Generalized State Space Averaging Method. IEEE Access. 2019;7:12241–51. https://doi.org/10.1109/access.2019.2891122.
22. Cheng H, Liu Y. Dynamic Modeling Framework for Evaluating Electromagnetic-Electro-Thermal Behavior of Power Conversion System During Load Operation. J Electron Packag. 2022. https://doi.org/10.1115/1.4055591.
23. Lin N, Cao S, Dinavahi V. Comprehensive Modeling of Large Photovoltaic Systems for Heterogeneous Parallel Transient Simulation of Integrated AC/DC Grid. IEEE Trans Energy Convers. 2020;35:917–27. https://doi.org/10.1109/tec.2020.2966729.
24. Fahim S, Hasanien H, Turky R, Aleem S, Ćalasan M. A Comprehensive Review of Photovoltaic Modules Models and Algorithms Used in Parameter Extraction. Energies. 2022. https://doi.org/10.3390/en15238941.
25. Gholami A, Ameri M, Zandi M, Ghoachani R. Electrical, thermal and optical modeling of photovoltaic systems: Step-by-step guide and comparative review study. Sustain Energy Technol Assess. 2022. https://doi.org/10.1016/j.seta.2021.101711.
26. Pedroza-Díaz A, Rodrigo P, Dávalos-Orozco Ó, De-La-Vega E, Valera-Albacete Á. Review of explicit models for photovoltaic cell electrical characterization. Renew Sustain Energy Rev. 2025. https://doi.org/10.1016/j.rser.2024.114979.
27. Wang G, Zhao K, Shi J, Zhang H, Yang X, Zhao Y. An iterative approach for modeling photovoltaic modules without implicit equations. Appl Energy. 2017;202:189–98. https://doi.org/10.1016/j.apenergy.2017.05.149.
28. Gu Z, Xiong G, Fu X. Parameter Extraction of Solar Photovoltaic Cell and Module Models with Metaheuristic Algorithms: A Review. Sustainability. 2023. https://doi.org/10.3390/su15043312.
29. Słowik A, Cpalka K, Xue Y, Hapka A. An efficient approach to parameter extraction of photovoltaic cell models using a new population-based algorithm. Appl Energy. 2024. https://doi.org/10.1016/j.apenergy.2024.123208.
30. Gholami A, Ameri M, Zandi M, Ghoachani R, Pierfederici S, Kazem H. Step-By-Step Guide to Model Photovoltaic Panels: An Up-To-Date Comparative Review Study. IEEE J Photovolt. 2022;12:915–28. https://doi.org/10.1109/jphotov.2022.3169525.
31. Chakraborty S, Wang J, Mahmud R, Hoke A, Johnson B, Bainy R, Lei H. Design of Multifunctional Electromagnetic Transient Model for Grid-Forming Inverters. IECON 2024–50th Annual Conf IEEE Industrial Electron Soc. 2024;1(6). https://doi.org/10.1109/iecon55916.2024.10905536
32. Choi J, Debnath S. (2021). Electromagnetic Transient (EMT) Simulation Algorithm for Evaluation of Photovoltaic (PV) Generation Systems. 2021 IEEE Kansas Power and Energy Conference (KPEC), 1–6. https://doi.org/10.1109/kpec51835.2021.9446234
33. Han Y, Lin X, Yang P, Xu L, Xu Y, Blaabjerg F. Structure-Preservation Model Aggregation for Two-Stage Inverters Based Large-Scale Photovoltaic System. IEEE Access. 2020;8:1824–39. https://doi.org/10.1109/access.2019.2962303.
34. Mundu M, Nnamchi S, Sempewo J, Uti DE. Simulation modeling for energy systems analysis: A critical review. Energy Inf. 2024;7(1):75. https://doi.org/10.1186/s42162-024-00374-8.
35. Nnamchi SN, Mundu MM, Ukagwu KJ, Oyagbola IA. Development and adaptation of relative sunshine hours models for the equatorial latitudes: a case study. Model Earth Syst Environ. 2022;8(1):1191–201. https://doi.org/10.1007/s40808-021-01147-y.
36. Choi J, Xue Y, Wang H. Electromagnetic Transient Simulation of Large-Scale Inverter-Based Resources With High-Granularity. IEEE Open Access J Power Energy. 2025;12:664–77. https://doi.org/10.1109/oajpe.2025.3615786.
37. Nnamchi SN, Nnamchi OA, Sanya OD, Mundu MM, Gabriel V. Dynamic analysis of performance of photovoltaic generators under moving cloud conditions. J Solar Energy Res. 2020;5(2):453–68. https://doi.org/10.22059/jser.2020.304561.1158.
38. Li M, Xiong L, Chai H, Xiu L, Hao J. Mechanism of PV Generation System Damping Electromechanical Oscillations. IEEE Access. 2020;8:135853–65. https://doi.org/10.1109/access.2020.3011456.
39. Wang Z. On the expanded Maxwell's equations for moving charged media system – General theory, mathematical solutions and applications in TENG. Mater Today. 2021. https://doi.org/10.1016/j.mattod.2021.10.027.
40. Kiap H, Aghaeiboorkheili M. The Foundation of Electromagnetism: A Comprehensive Study of Maxwell's Equations. Afr J Math Stat Stud. 2025. https://doi.org/10.52589/ajmss-dbspwnno.
41. Jin S, Liu N,C. Quantum simulation of Maxwell's equations via Schrödingerisation. ESAIM: Math Modelling Numer Anal. 2023. https://doi.org/10.1051/m2an/2024046.
42. Li X, Hylton N, Giannini V, Lee K, Ekins-Daukes N, Maier S Multi-dimensional modeling of solar cells with electromagnetic and carrier transport calculations. Prog Photovoltaics Res Appl. 2013;21. https://doi.org/10.1002/pip.2159.
43. Shi Q, Zhuang C, Liu J, Lin B, Peng X, Wu D, Liu Z, Zeng R. Hybrid-Parallel Collaborative Simulation Framework Integrating Device Physics With Circuit Dynamics for PDAE-Modeled Power Electronic Equipment. IEEE Trans Power Electron. 2025;40:8168–78. https://doi.org/10.1109/tpel.2025.3534030.
44. Yao Y, Wang Y, Jia H, Mu Y. An analytical approach based on coupled multi-physics model for photovoltaic arrays performance simulation. Electr Power Syst Res. 2023. https://doi.org/10.1016/j.epsr.2023.109773.
45. Chen P, Han J, Yao X, Wang X, Yan Y, Zhao Z, Zhang L, Yu Z, Li H. Modeling and Testing of 3D Wound Core Loss of Amorphous Alloy Transformer for Photovoltaic Inverter. Energies. 2025. https://doi.org/10.3390/en18112698.
46. Li F, Wu W. Coupled electrical-thermal performance estimation of photovoltaic devices: A transient multiphysics framework with robust parameter extraction and 3-D thermal analysis. Appl Energy. 2022. https://doi.org/10.1016/j.apenergy.2022.119249.
47. Siddiqui M, Siddiqui O, Alquaity A, Ali H, Arif A, Zubair S. A comprehensive review on multi-physics modeling of photovoltaic modules. Energy Conv Manag. 2022. https://doi.org/10.1016/j.enconman.2022.115414.
48. Berchenko-Kogan Y, Stern A. Constraint-Preserving Hybrid Finite Element Methods for Maxwell's Equations. Found Comput Math. 2019;21:1075–98. https://doi.org/10.1007/s10208-020-09476-7.

49. Kozioł M. Reevaluation and correction of Maxwell's Equations: a magnetic field has a source, a moving electric charge. F1000Research. 2020;9:1092. https://doi.org/10.12688/f1000research.26035.1.
50. Reggia J Generalizing Maxwell's equations to complex-valued electromagnetic fields. Phys Scr. 2023;99. https://doi.org/10.1088/1402-4896/ad10dc.
51. Tan E. (2025). On the Unification of Electrostatics and Magnetostatics via Maxwell's Eq. 2025 IEEE Wireless Antenna and Microwave Symposium (WAMS), 1–3. https://doi.org/10.1109/wams64402.2025.11158540
52. Coetzer K, Rix A, Wiid P. Measurement-Based Nonlinear SPICE-Compatible Photovoltaic Models for Simulating the Effects of Surges and Electromagnetic Interference within Installations. Energies. 2022. https://doi.org/10.3390/en15218162.
53. Bermúdez A, Gómez D, Martínez I. A comparison of lumped parameter models and Maxwell's equations for wireless power transfer. SeMA J. 2025. https://doi.org/10.1007/s40324-025-00405-8.
54. Adak S Control strategy evaluation for reactive power management in grid-connected photovoltaic systems under varying solar conditions. Sci Rep. 2025;15. https://doi.org/10.1038/s41598-025-08918-y.
55. Beinert A, Romer P, Heinrich M, Aktaa J, Neuhaus H. Thermomechanical design rules for photovoltaic modules. Prog Photovoltaics Res Appl. 2022;31:1181–93. https://doi.org/10.1002/pip.3624.
56. Bosco N, Springer M, He X. Viscoelastic Material Characterization and Modeling of Photovoltaic Module Packaging Materials for Direct Finite-Element Method Input. IEEE J Photovolt. 2020;10:1424–40. https://doi.org/10.1109/jphotov.2020.3005086.
57. El-Hamid A, Wei G. Effect of varying the thermophysical properties of phase change material on the performance of photovoltaic/thermal-PCM hybrid module numerically. J Energy Storage. 2024. https://doi.org/10.1016/j.est.2024.111326.
58. Lopez-Richard V, Meneghetti L, Nogueira G, Hartmann F, Graeff C. Unified model for probing solar cell dynamics via cyclic voltammetry and impedance spectroscopy. Phys Rev B. 2024. https://doi.org/10.1103/physrevb.110.115306.
59. Harrison A. PILoN: Physics-informed logistic nonlinear model for photovoltaic performance modelling. Energy Rep. 2026;15:109026.
60. Santos L, Alskaif T, Barroso G, Carvalho P. Photovoltaic power estimation and forecast models integrating physics and machine learning: A review on hybrid techniques. Sol Energy. 2024. https://doi.org/10.1016/j.solener.2024.113044.
61. Santos L, Alskaif T, Carvalho P Hybrid Models for Photovoltaic Power Forecasting under Different Physical Modeling Approaches. 2025 IEEE Kiel PowerTech. 2025;1–6. https://doi.org/10.1109/powertech59965.2025.11180736.
62. Yu X, Xia Y, Wang Z. (2024). Combining Physical Mechanisms with Data-Driven Approaches for Short-Term Photovoltaic Power Forecasting. 2024 IEEE 8th Conference on Energy Internet and Energy System Integration (EI2), 4482–4487. https://doi.org/10.1109/ei264398.2024.10990413
63. Jahangir J, Alam M. Physics-guided machine learning predicts the planet-scale performance of solar farms with sparse, heterogeneous, public data. ArXiv. 2024. https://doi.org/10.48550/arxiv.2407.18284. abs/2407.18284.
64. De Barandja DB, Pakouzou V, Ramde B, M'boliguipa E, Saria J, Zoungrana M, M., Zerbo I. Modeling the response of an illuminated polysilicon solar cell under the influence of radio waves, a 3D approach. Energy Rep. 2021;7:2094–100. https://doi.org/10.1016/j.egyr.2021.04.015.
65. Oni A, Mohsin A, Rahman M, Bhuian M. A comprehensive evaluation of solar cell technologies, associated loss mechanisms, and efficiency enhancement strategies for photovoltaic cells. Energy Rep. 2024. https://doi.org/10.1016/j.egyr.2024.03.007.
66. Ouédraogo A, Savadogo M, Honadia P, Bathiébo D, Kam S. Individual Energetic Processes Efficiencies in a Polycrystalline Silicon PV Cell Versus Electromagnetic Field. Silicon. 2021;14:7005–15. https://doi.org/10.1007/s12633-021-01480-y.
67. Ouédraogo A, Soro B, Konaté R, Oumarou F, Bathiébo D. Investigation of the Polycrystalline Silicon PV Cell Efficiency in 3D Approximation versus Electromagnetic Field under Monochromatic Illumination. Int J Photoenergy. 2021. https://doi.org/10.1155/2021/5171351.
68. Qiu W, Zhang L, Yin H, Markel L, Liao D, McConnell B, Liu Y. Modeling, testing, and mitigation of electromagnetic pulse on PV systems. Sol Energy. 2023. https://doi.org/10.1016/j.solener.2023.112010.
69. Saria M, Zouma B, Korgo B, De Dieu Bokoyo Barandja V, Zoungrana M, Zerbo I, Bathiébo D. Effect of Reverse Polarisation of an Electromagnetic Field on the Performance of a Silicon PV Cell. Adv Mater Sci Eng. 2020. https://doi.org/10.1155/2020/1320268.
70. Zinßer M, Helder T, Bauer A, Friedlmeier T, Zillner J, Becker J, Powalla M. Optical and Electrical Loss Analysis of Thin-Film Solar Cells Combining the Methods of Transfer Matrix and Finite Elements. IEEE J Photovolt. 2022;12:1154–61. https://doi.org/10.1109/jphotov.2022.3190770.
71. Lee S, Jo H, So M, Sohn C, Han I, Kim J, Bae I, Lee S, Noh S, Choi H, Leem J. Investigation of internal electric fields in GaAs solar cell under highly-concentrated light. J Korean Phys Soc. 2015;66:667–71. https://doi.org/10.3938/jkps.66.667.
72. Marsh R, Hodgkiss J, Friend R Direct Measurement of Electric Field-Assisted Charge Separation in Polymer:Fullerene Photovoltaic Diodes. Adv Mater. 2010;22. https://doi.org/10.1002/adma.201001010.
73. Moia D, Gelmetti I, Calado P, Hu Y, Li X, Docampo P, De Mello J, Maier J, Nelson J, Barnes P. Dynamics of Internal Electric Field Screening in Hybrid Perovskite Solar Cells Probed Using Electroabsorption. Phys Rev Appl. 2022. https://doi.org/10.1103/physrevapplied.18.044056.
74. Hashemi B, Taheri S, Crétu A, Pouresmaeil E. Systematic photovoltaic system power losses calculation and modeling using computational intelligence techniques. Appl Energy. 2021. https://doi.org/10.1016/j.apenergy.2020.116396.
75. Ramirez A, Vargas U, Abdel-Rahman M. Lumped-parameters equivalent of a photovoltaic system for load flow analysis. Renewable Energy. 2021. https://doi.org/10.1016/j.renene.2021.01.105.
76. Zou W, Yu G, Du X. Energy and exergy analysis of photovoltaic thermal collectors: Comprehensive investigation of operating parameters in different dynamic models. Renewable Energy. 2024. https://doi.org/10.1016/j.renene.2023.119710.
77. Bu C, Zhang Z, Hou T, Bai X, He H Research on Electromagnetic Compatibility of High Frequency Switching Power Supply Based on Harmonic Balance Finite Element Method. J Phys: Conf Ser. 2021;2132. https://doi.org/10.1088/1742-6596/2132/1/012041.
78. Kharanaq F, Emadi A, Bilgin B. Modeling of Conducted Emissions for EMI Analysis of Power Converters: State-of-the-Art Review. IEEE Access. 2020;8:189313–25. https://doi.org/10.1109/access.2020.3031693.
79. Takahashi S, Wada K, Ayano H, Ogasawara S, Shimizu T. Review of Modeling and Suppression Techniques for Electromagnetic Interference in Power Conversion Systems. IEEJ J Ind Appl. 2021. https://doi.org/10.1541/ieejjia.21006800.

80. Hasan M, Abu-Siada A, Islam S, Dahidah M. A New Cascaded Multilevel Inverter Topology with Galvanic Isolation. IEEE Trans Ind Appl. 2018;54:3463–72. https://doi.org/10.1109/tia.2018.2818061.
81. Karthik A, Loganathan U. A Reduced Component Count Five-Level Inverter Topology for High Reliability Electric Drives. IEEE Trans Power Electron. 2020;35:725–32. https://doi.org/10.1109/tpel.2019.2913821.
82. Chen Q, Zhang Y, Huang P, Chen Q, Yang Z, Jiang Y, Optical Electrical, Thermal, Stress, and Energy Yield Simulations Enhance the Performance and Stability of Perovskite Photovoltaics. Adv Mater. 2025;38. https://doi.org/10.1002/adma.202514184.
83. Fan X, Li D, Kong W, Cao L, Qu R, Yin Z. Fast Calculation of Strand Eddy Current Loss in Inverter-Fed Electrical Machines. IEEE Trans Industr Electron. 2023;70:4640–50. https://doi.org/10.1109/tie.2022.3183338.
84. Hai-Sen Z, Dongdong Z, Yilong W, Yang Z, Guorui X. Piecewise Variable Parameter Loss Model of Laminated Steel and Its Application in Fine Analysis of Iron Loss of Inverter-Fed Induction Motors. IEEE Trans Ind Appl. 2016;54:832–40. https://doi.org/10.1109/ias.2016.7731912.
85. Zhang D, Yi J, Zhu H, Ahmad T, Zhao H, Goh H, Zhang Y, Wu T. The Electromagnetic Losses Analysis of Inverter-Fed Induction Motor Accounting for Interbar Current and Rotor Slip Frequency. IEEE Trans Transp Electrification. 2022;8:1155–67. https://doi.org/10.1109/tte.2021.3104400.
86. Ge C, Duan B, Lou S, Qian S, Wang W. On Improving Convergence Characterization to Solve the Electromagnetic–Thermal Model. IEEE Trans Microwave Theory Tech. 2021;69:3624–34. https://doi.org/10.1109/tmtt.2021.3076211.
87. Lanteri S, Scheid C, Viquerat J Analysis of a Generalized Dispersive Model Coupled to a DGTD Method with Application to Nanophotonics. SIAM J Sci Comput. 2017;39. https://doi.org/10.1137/15m105207x.
88. Roth T, Chew W. Stability analysis and discretization of A-Φ time domain integral equations for multiscale electromagnetics. J Comput Phys. 2020;408:109102. https://doi.org/10.1016/j.jcp.2019.109102.

Publisher's Note

Springer Nature remains neutral with regard to jurisdictional claims in published maps and institutional affiliations.